

Color image restoration with impulse noise based on fractional-order total variation and framelet

R. Parvaz*

Department of Mathematics, University of Mohaghegh Ardabili, 56199-11367
Ardabil, Iran.

Abstract

Restore lost images due to noise and blurred is a burgeoning subject in image processing and despite the different algorithms on this subject, but the effort to improve is always considered. The definition of fractional derivatives in recent years has created a powerful tool for this purpose. In the present paper, using fractional-order total variation and framelet transform, the nonconvex model for image restoration with impulse noise problem is improved. Then by alternating direction method of multipliers (ADMM) and primal-dual problem, the proposed model is solved. The convergence of the proposed algorithm is studied. And the proposed algorithm is evaluated using different types of tests. The output results show the efficiency of proposed method.

Keywords: Image deblurring; Fractional total variation; Framelet; Nonconvex.

1 Introduction

The image blurring and noise process can be considered by using the following formula

$$F = h \circledast U + N_\epsilon,$$

where F and $U \in \mathbb{R}^{n \times m}$ are observed and original images, respectively, and N_ϵ shows noise. Also, $h \in \mathbb{R}^{r \times s}$ is blurred kernel and \circledast denotes two-dimensional convolution operator. The above relation can be rewritten as a linear equation as follows

$$f = Au + n_\epsilon,$$

where f and $u \in \mathbb{R}^{nm \times 1}$ denote the reshaped of observed and original images, respectively. Also $A \in \mathbb{R}^{nm \times nm}$ is obtained according to the blurred kernel and boundary conditions for the blurred process. There are four main boundary conditions

*Corresponding author, Email: reza.parvaz@yahoo.com, rparvaz@uma.ac.ir

that include zero, periodic, reflexive and anti-reflexive boundary conditions. Depending on each of these boundary conditions, the matrix A has a special structure. For example in the zero boundary condition, A is a block toeplitz with toeplitz blocks (BTTB) matrix or in the periodic boundary condition, A is a block circulant with circulant blocks (BCCB) matrix. Due to the noise and large size of the unknown coefficients and ill-conditioned for this linear equation, it is not possible to solve this problem directly. The first attempts to solve this problem can be made on SVD decompositions. But in most cases, this method does not have the desired output. Other method, that can be used for this problem is the basis pursuit problem [5] by minimization problem as

$$\min_u \{\|u\|_1 : Au = f\},$$

which is studied in many papers as [26, 35]. One of the most popular methods that has attracted the most attention is the use of total variation (TV) based on regularization scheme (the ROF model). This model is introduced by Rudin, Osher, and Fatemi [25] as

$$\min_u \frac{\lambda}{2} \|Au - f\|_2^2 + \int_{\Omega} |Du|,$$

where Ω shows a bounded open subset with Lipschitzian boundary in \mathbb{R}^2 and Du denotes the derivative of u . The idea of using total variation has been considered in recent years and has been used in various articles, for example [24, 1, 19, 32]. One of the most important tools that has improved this method in recent years is the use of fractional derivatives. Despite the existence of different definitions for fractional derivatives, such as Riemann-Liouville (R-L) and Caputo definition, the Grünwald-Letnikov (G-L) definition is often used in image processing due to its lower computational complexity than other definitions. Based on these types of derivatives, fractional-order total variation (FTV) is introduced and used in image and signal processing [16, 22, 6]. With the development of the wavelet and framelet concept, an efficient tool for image and signal processing is developed that has been used in various articles as [4, 13, 3, 17]. These concepts are introduced in the following subsections. The reader can find more information about these concepts in [12, 28, 11]. The l_1 norm based on frame transform for restoration problem is introduced by Dong, Ji and Shen [7]. Due to the structure of l_1 norm as nonsmooth and nonseparable, solving a problem that includes these norms is hard. The split Bregman algorithm is a suitable tool for solving these types of problems [29, 36, 14]. In the proposed model a non-convex $(l_1 - l_2)$ -norm is considered as regularization term. $(l_1 - l_2)$ -norm is studied in many papers as [18, 21]. Also, this norm based on frame transform is used by Jingjing Liu et al in [18] as following model

$$\min_u \|Au - f\|_1 + \lambda_1 (\|Wu\|_1 - \beta \|u\|_2),$$

where W represent the matrix of framelet transform. As it is clear from this model, the total variation phrase is not observed in this model. Therefore, adding this expression can improve the algorithm. Total variation method can preserve edges very

well in the restored image, then this helps to improve the restored image. Although the ordinary method of minimization is slow for this problem [2, 33], the optimal algorithm based on primal-dual is introduced for solving this problem in [34, 10, 8, 9].

The organization of this paper is as follows: In Section 2, the tools used in the proposed algorithm briefly introduced. The details of the proposed method are given in Section 3. The convergence analysis of the proposed algorithm is given in Section 4. Simulation results and algorithm analysis are studied in Section 5. Also the summary of paper is given in Section 6.

2 Preliminaries

Definition 2.1. Let \mathcal{H} be a separable Hilbert space. Then the sequence $F = \{f_i\}_{i \in I} \subseteq \mathcal{H}$ is named a frame in \mathcal{H} if there exist two constants as ρ_1 and ρ_2 such that for all $f \in \mathcal{H}$

$$\rho_1 \|f\|^2 \leq \sum_{i \in I} |\langle f, f_i \rangle|^2 \leq \rho_2 \|f\|^2.$$

When $\rho_1 = \rho_2 = 1$, frame is called a Parseval frame in $\mathcal{H} = L_2(\mathbb{R})$.

In this paper, particular Parseval framelet systems in \mathcal{H} that are constructed by B-spline whose refinement mask is $h_0 = \frac{1}{4}[1, 2, 1]$, with two corresponding framelet masks $h_1 = \frac{\sqrt{2}}{4}[1, 0, -1]$ and $h_2 = \frac{1}{4}[-1, 2, -1]$. Complete information about frame and framelet is available in [12, 28, 11], and the reader can refer to these sources.

Definition 2.2. The G-L fractional-order derivatives D_x^α and D_y^α for input image u of order $\alpha \in \mathbb{R}^+$ are defined as

$$D_x^\alpha u_{i,j} := \sum_{l=0}^{k-1} \phi_l^\alpha u_{i-k,l},$$

$$D_y^\alpha u_{i,j} := \sum_{l=0}^{k-1} \phi_l^\alpha u_{i,j-k,l},$$

where $\phi_l^\alpha = (-1)^l \frac{\Gamma(\alpha+1)}{\Gamma(l+1)\Gamma(\alpha+1-l)}$ and k denotes the number of neighboring pixels. Also the discrete fractional-order gradient is considered as $\nabla^\alpha u = [D_x^\alpha u, D_y^\alpha u]^T$.

Definition 2.3. The adjoint operators of the fractional-order derivatives are defined as

$$(D_x^\alpha)^T u_{i,j} := \sum_{l=0}^{k-1} \phi_l^\alpha u_{i+k,l},$$

$$(D_y^\alpha)^T u_{i,j} := \sum_{l=0}^{k-1} \phi_l^\alpha u_{i,j+k,l}.$$

Based on above definitions for a vector function $\mathbf{p}(x, y) = (p_1(x, y), p_2(x, y))$ the fractional divergence operator can be obtained as

$$div^\alpha \mathbf{p} = (-1)^\alpha (\nabla^\alpha)^T \mathbf{p} = (-1)^\alpha ((D_x^\alpha)^T p_{i,j}^1 + (D_y^\alpha)^T p_{i,j}^2).$$

3 Proposed minimization model and iterative method

3.1 Proposed model

In the proposed model, the following model based on FTV is introduced for restoration of image with impulse noise

$$\min_u \|Au - f\|_1 + \lambda_1 (\|Wu\|_1 - \beta \|u\|_2) + \lambda_2 \|u\|_{FTV}, \quad (3.1)$$

where λ_1, λ_2 and β are positive given parameters. Also $\|\cdot\|_{FTV}$ denotes fractional-order total variation norm that defined as

$$\|u\|_{FTV} = \sum_{i,j} \sqrt{(D_x^\alpha u_{i,j})^2 + (D_y^\alpha u_{i,j})^2}.$$

This model contains a nonconvex sentence. There are several methods for solving nonconvergent optimization problems, for example see [23]. In the proposed method, alternating direction method of multipliers (ADMM) is used for solving this problem. By auxiliary variables $m = \{m_i\}_{i=1}^3$, (3.1) can be written as

$$\begin{aligned} \min_u \|m_1\|_1 + \lambda_1 (\|m_2\|_1 - \beta \|u\|_2) + \lambda_2 \|m_3\|_{FTV}, \\ \text{s.t. } m_1 = Au - f, \quad m_2 = Wu, \quad m_3 = u. \end{aligned} \quad (3.2)$$

The augmented Lagrangian for (3.2) is obtained as

$$\begin{aligned} \min_{u, m, n} L(u, m_1, m_2, m_3, n_1, n_2, n_3) = \min_{u, m, n} \|m_1\|_1 + \lambda_1 (\|m_2\|_1 - \beta \|u\|_2) + \lambda_2 \|m_3\|_{FTV} \\ + \mu_1 \langle Au - f - m_1, n_1 \rangle + \frac{\mu_1}{2} \|Au - f - m_1\|_2^2 + \mu_2 \langle Wu - m_2, n_2 \rangle \\ + \frac{\mu_2}{2} \|Wu - m_2\|_2^2 + \mu_3 \langle u - m_3, n_3 \rangle + \frac{\mu_3}{2} \|u - m_3\|_2^2, \end{aligned} \quad (3.3)$$

where $n = \{n_i\}_{i=1}^3$ and $\mu_i > 0$, $i = 1, 2, 3$ are the Lagrange multipliers and penalty parameters, respectively. The extended iterative algorithm for solving problem (3.3) based on ADMM is given as

$$\begin{aligned} u^{k+1} = \arg \min_u -\lambda_1 \beta \|u\|_2 + \mu_1 \langle Au - f - m_1^k, n_1^k \rangle + \frac{\mu_1}{2} \|Au - f - m_1^k\|_2^2 \\ + \mu_2 \langle Wu - m_2^k, n_2^k \rangle + \frac{\mu_2}{2} \|Wu - m_2^k\|_2^2 + \mu_3 \langle u - m_3^k, n_3^k \rangle \\ + \frac{\mu_3}{2} \|u - m_3^k\|_2^2, \end{aligned} \quad (3.4)$$

$$m_1^{k+1} = \arg \min_{m_1} \|m_1\|_1 + \mu_1 \langle Au^{k+1} - f - m_1, n_1^k \rangle + \frac{\mu_1}{2} \|Au^{k+1} - f - m_1\|_2^2, \quad (3.5)$$

$$n_1^{k+1} = n_1^k + Au^{k+1} - f - m_1^{k+1}, \quad (3.6)$$

$$m_2^{k+1} = \arg \min_{m_2} \lambda_1 \|m_2\|_1 + \mu_2 \langle Wu^{k+1} - m_2, n_2^k \rangle + \frac{\mu_2}{2} \|Wu^{k+1} - m_2\|_2^2, \quad (3.7)$$

$$n_2^{k+1} = n_2^k + Wu^{k+1} - m_2^{k+1}, \quad (3.8)$$

$$m_3^{k+1} = \arg \min_{m_3} \lambda_2 \|m_3\|_{FTV} + \mu_3 \langle u^{k+1} - m_3, n_3^k \rangle + \frac{\mu_3}{2} \|u^{k+1} - m_3\|_2^2, \quad (3.9)$$

$$n_3^{k+1} = n_3^k + u^{k+1} - m_3^{k+1}. \quad (3.10)$$

3.2 Solve subproblems

In this subsection, the solution to each of the subproblems introduced in the previous subsection are studied. For (3.4) by using the optimal condition, we get

$$\begin{aligned} & (\mu_1 A^T A + \mu_3 I + \mu_2 I - \lambda_1 \beta / \|u^k\|_2 I) u \\ & = \mu_1 A^T (f + m_1^k - n_1^k) + \mu_2 W^T (m_2^k - n_2^k) + \mu_3 (m_3^k - n_3^k). \end{aligned} \quad (3.11)$$

Under the periodic condition for blurred processing, the blurred matrix can be generated as block circulant with circulant blocks (BCCB) matrix. It is well known in the field of linear algebra that these types of matrices are decomposed using Fourier transform. And due to the fast Fourier transform (FFT), the calculation is performed faster. So by considering the periodic condition, Eq. (3.11) is changed as

$$\begin{aligned} & (\mu_1 \Lambda^* \Lambda + (\mu_3 + \mu_2 - \lambda_1 \beta / \|u^k\|_2) I) F u^{k+1} \\ & = \mu_1 \Lambda^* F (f + m_1^k - n_1^k) + \mu_2 F W^T (m_2^k - n_2^k) + \mu_3 F (m_3^k - n_3^k), \end{aligned} \quad (3.12)$$

where $*$ and F denote the complex conjugacy and fast Fourier transform, respectively. Also Λ is a diagonal matrix dependent on the eigenvalues of the blurred matrix. The equation (3.12) can be easily solved using Fourier calculations.

Subproblem (3.5) can be rewritten as

$$m_1^{k+1} = \arg \min_{m_1} \|m_1\|_1 + \frac{\mu_1}{2} \|m_1 - (Au^{k+1} - f + n_1^k)\|_2^2.$$

The solution for the above problem based on proximal mapping for l_1 -norm can be obtained as

$$m_1^{k+1} = \Psi_{1/\mu_1}(Au^{k+1} - f + n_1^k), \quad (3.13)$$

where Ψ is defined as

$$\Psi_a(x) = \text{sign}(x) \max(|x| - a, 0).$$

In a similar way, (3.7) can be written as

$$m_2^{k+1} = \arg \min_{m_2} \lambda_1 \|m_2\|_1 + \frac{\mu_2}{2} \|m_2 - (Wu^{k+1} + n_2^k)\|_2^2,$$

and the solution by proximal mapping is earned as

$$m_2^{k+1} = \Psi_{\lambda_1/\mu_2}(Wu^{k+1} + n_2^k). \quad (3.14)$$

In order to avoid complex calculations for Eq. (3.9), the dual problem is used to find the solution. In the first step, Eq. (3.9) is changed as

$$m_3^{k+1} = \operatorname{argmin}_{m_3} \lambda_2 \|m_3\|_{FTV} + \frac{\mu_3}{2} \|m_3 - (u^{k+1} - n_3^k)\|_2^2, \quad (3.15)$$

then in the next step, the dual problem is obtained and solved for this problem.

Lemma 3.1. *If we consider $J(u) = \min_u \|u\|_{FTV}$ then the dual problem of $J(u)$ is obtained as [8]*

$$J(u) = \sup_{\mathbf{p}} \langle \mathbf{p}, \nabla^\alpha u \rangle - J^*(\mathbf{p}),$$

where

$$J^*(\mathbf{p}) = \begin{cases} 0, & \text{if } |\mathbf{p}| \leq 1, \\ \infty, & \text{if } |\mathbf{p}| > 1. \end{cases}$$

Based on Lemma 3.1, the corresponding primal-dual problem of (3.15) is written as follows

$$(m_3^{k+1}, \mathbf{p}^{k+1}) = \operatorname{argmin}_{m_3} \max_{\mathbf{p} \in \chi} \frac{\lambda_2}{\mu_3} \langle \mathbf{p}, \nabla^\alpha m_3 \rangle + \frac{1}{2} \|m_3 - (u^{k+1} - n_3^k)\|_2^2, \quad (3.16)$$

where $\chi = \{\mathbf{p} \in \mathbb{R}^{2nm} | \mathbf{p}_i \in \mathbb{R}^2, \|\mathbf{p}_i\|_2 \leq 1, \forall i \in \{1, \dots, nm\}\}$. By the iterative scheme, the solution of the primal-dual problem (3.16) can be written as

$$\mathbf{p}^{k+1} = \operatorname{argmax}_{\mathbf{p} \in \chi} \frac{\lambda_2}{\mu_3} \langle \mathbf{p}, \nabla^\alpha \hat{m}_3^k \rangle - \frac{1}{2\gamma} \|\mathbf{p} - \mathbf{p}^k\|_2^2, \quad (3.17)$$

$$m_3^{k+1} = \operatorname{argmin}_{m_3} \frac{\lambda_2}{\mu_3} \langle \mathbf{p}^{k+1}, \nabla^\alpha m_3 \rangle + \frac{1}{2} \|m_3 - (u^{k+1} - n_3^k)\|_2^2, \quad (3.18)$$

$$\hat{m}_3^{k+1} = 2m_3^{k+1} - m_3^k. \quad (3.19)$$

After simplifying (3.17)-(3.18), the following statements are obtained

$$\mathbf{p}^{k+1} = \frac{\mathbf{p}^k + \frac{\lambda_2\gamma}{\mu_3} \nabla^\alpha \hat{m}_3^k}{\max(|\mathbf{p}^k + \frac{\lambda_2\gamma}{\mu_3} \nabla^\alpha \hat{m}_3^k|, 1)}, \quad (3.20)$$

$$m_3^{k+1} = m_3^k - \tau \left(\frac{\lambda_2\gamma}{\mu_3} (\nabla^\alpha)^T \mathbf{p}^{k+1} + m_3^k - (u^{k+1} - n_3^k) \right), \quad (3.21)$$

where τ is step size and γ is a positive constant.

The general structure of the proposed method for restoration of blurred images with impulse noise is summarized in Algorithm 1.

Algorithm 1: Restoration proposed algorithm.

Initialization: $\alpha, \beta, \tau, \gamma, \{\lambda_i\}_{i=1}^2, \{\mu_i\}_{i=1}^3, m^0, n^0, u^0$.
for $k=1, \dots$ **do**
 Compute u^k by solving (3.12),
 Compute m_1^k by solving (3.13),
 Compute n_1^k by solving (3.6),
 Compute m_2^k by solving (3.14),
 Compute n_2^k by solving (3.8),
 Compute m_3^k by solving (3.19)-(3.21),
 Compute n_3^k by solving (3.10),
end for
If the stop condition is met in the above step, stop the loop.

3.3 Extended algorithm for color image

The proposed restoration algorithm for grayscale image is introduced in the previous subsection. But this algorithm can be extended to color images. In the following, the details of the proposed algorithm for color images are explained. The blurred matrix for color image is given in $\mathbb{R}^{3nm \times 3nm}$ as

$$A = \begin{bmatrix} A_{rr} & A_{rg} & A_{rb} \\ A_{gr} & A_{gg} & A_{gb} \\ A_{br} & A_{bg} & A_{bb} \end{bmatrix}.$$

Also, in the calculations related to this subsection, for different layers of the color image, we expand the values that is calculated in the previous subsection as $u = [u_r; u_g; u_b]$, $f = [f_r; f_g; f_b]$, $m_i = [m_{i,r}; m_{i,g}; m_{i,b}]$, $n_i = [n_{i,r}; n_{i,g}; n_{i,b}]$ for $i = 1, 2, 3$. Using the same procedure mentioned in the pervious section the following phrase is obtained

$$\begin{aligned} & (\mu_1 \Lambda^* \Lambda + (\mu_3 + \mu_2 - \lambda \beta / \|u\|_2) I) \hat{F} u^{k+1} \\ & = \mu_1 \Lambda^* \hat{F} (f + m_1^k - n_1^k) + \mu_2 \hat{F} W^T (m_2^k - n_2^k) + \mu_3 \hat{F} (m_3^k - n_3^k), \end{aligned} \quad (3.22)$$

where $\hat{F} = I \otimes F$, here \otimes shows the Kronecker product. Also Λ is obtained after decomposed using Fourier transform as

$$\Lambda = \begin{bmatrix} \Lambda_{rr} & \Lambda_{rg} & \Lambda_{rb} \\ \Lambda_{gr} & \Lambda_{gg} & \Lambda_{gb} \\ \Lambda_{br} & \Lambda_{bg} & \Lambda_{bb} \end{bmatrix}.$$

Other parts of the proposed algorithm are similar to those described in the pervious section, and the calculation details are given in Algorithm 2. The simulation results of the algorithms described in this section are studied in the simulation results section.

Algorithm 2: Color image restoration proposed algorithm.

Initialization: $\alpha, \beta, \tau, \gamma, \{\lambda_i\}_{i=1}^2, \{\mu_i\}_{i=1}^3, m^0, n^0, u^0$.

for $k=1, \dots$ **do**

 Compute u^k by solving (3.22),

for $l=r, g, b$ **do**

 Compute $m_{1,l}^k$ by solving: $m_{1,l}^k = \Psi_{1/\mu_1}(Au_l^k - f_l + n_{1,l}^{k-1})$,

 Compute $n_{1,l}^k$ by solving: $n_{1,l}^k = n_{1,l}^{k-1} + Au_l^k - f - m_{1,l}^k$,

 Compute $m_{2,l}^k$ by solving: $m_{2,l}^k = \Psi_{\lambda_1/\mu_2}(Wu_l^k + n_{2,l}^{k-1})$,

 Compute $n_{2,l}^k$ by solving: $n_{2,l}^k = n_{2,l}^{k-1} + Wu_l^k - m_{2,l}^k$,

 Compute $m_{3,l}^k$ by solving:

$$\mathbf{p}_l^k = \frac{\mathbf{p}_l^{k-1} + \frac{\lambda_2 \gamma}{\mu_3} \nabla^\alpha \hat{m}_{3,l}^{k-1}}{\max(\mathbf{p}_l^{k-1} + \frac{\lambda_2 \gamma}{\mu_3} \nabla^\alpha \hat{m}_{3,l}^{k-1}, 1)},$$

$$m_{3,l}^k = m_{3,l}^{k-1} - \tau \left(\frac{\lambda_2 \gamma}{\mu_3} (\nabla^\alpha)^T \mathbf{p}_l^k + m_{3,l}^{k-1} - (u_l^k + n_{3,l}^{k-1}) \right),$$

$$\hat{m}_{3,l}^k = 2m_{3,l}^k - m_{3,l}^{k-1},$$

 Compute $n_{3,l}^k$ by solving: $n_{3,l}^k = n_{3,l}^{k-1} + u_l^k - m_{3,l}^k$,

end for

end for

If the stop condition is met in the above step, stop the loop.

4 Convergence analysis

In this section, the convergence of the proposed method is studied. The convergence analysis for proposed method is based on the described method in [18, 21].

Lemma 4.1. *Let the objective function be increasing, that is $\|Au - f\|_1 + \lambda_1(\|Wu\|_1 - \beta\|u\|_2) + \lambda_2\|u\|_{FTV} \rightarrow \infty$ when $\|x\|_2 \rightarrow \infty$. Also assume that $\{u^k, m_1^k, m_2^k, m_3^k, n_1^k, n_2^k, n_3^k\}$ be the sequence generated by the proposed method, then the following statements hold:*

a)

$$\begin{aligned} & L(u^{k+1}, m_1^{k+1}, m_2^{k+1}, m_3^{k+1}, n_1^{k+1}, n_2^{k+1}, n_3^{k+1}) - L(u^k, m_1^k, m_2^k, m_3^k, n_1^k, n_2^k, n_3^k) \\ & \leq \sum_{i=1}^3 C_i \|m_i^{k+1} - m_i^k\|_2^2. \end{aligned}$$

b) If there exists a $p \in \partial_u L(u^{k+1}, m_1^{k+1}, m_2^{k+1}, m_3^{k+1}, n_1^{k+1}, n_2^{k+1}, n_3^{k+1})$ then

$$\begin{aligned} & \|p\|_2 + \sum_i^3 (\partial_{m_i} + \partial_{n_i}) L(u^{k+1}, m_1^{k+1}, m_2^{k+1}, m_3^{k+1}, n_1^{k+1}, n_2^{k+1}, n_3^{k+1}) \\ & \leq \sum_{i=1}^3 C_{i+3} \|m_i^{k+1} - m_i^k\|_2, \end{aligned}$$

where in conditions (a) and (b), $\{C_i\}_{i=1}^6$ are constant.

Proof. a) By problem (3.4), we get

$$L(u^{k+1}, m_1^k, m_2^k, m_3^k, n_1^k, n_2^k, n_3^k) - L(u^k, m_1^k, m_2^k, m_3^k, n_1^k, n_2^k, n_3^k) \leq 0.$$

Also by using (3.5)-(3.10), we obtain

$$\begin{aligned} & L(u^{k+1}, m_1^{k+1}, m_2^{k+1}, m_3^{k+1}, n_1^{k+1}, n_2^{k+1}, n_3^{k+1}) - L(u^k, m_1^k, m_2^k, m_3^k, n_1^k, n_2^k, n_3^k) \\ & \leq \|m_1^{k+1}\|_1 - \|m_1^k\|_1 + \lambda_1(\|m_2^{k+1}\|_1 - \|m_2^k\|_1) + \lambda_2(\|m_3^{k+1}\|_{FTV} - \|m_3^k\|_{FTV}) \\ & + \sum_{i=3}^3 \mu_i(\|n_i^{k+1} - n_i^k\|_2^2 - \langle n_i^k, m_i^{k+1} - m_i^k \rangle - \frac{1}{2}\|m_i^{k+1} - m_i^k\|_2^2 \\ & - \langle m_i^{k+1} - m_i^k, n_i^{k+1} - n_i^k \rangle). \end{aligned}$$

Based on optimality conditions for (3.5)-(3.10), we have $\partial_{m_1} \|m^{k+1}\|_1 = \mu_1 n_1^{k+1}$, $\lambda_1 \partial_{m_2} \|m_2^{k+1}\|_1 = \mu_2 n_2^{k+1}$ and $\lambda_2 \partial_{m_3} \|m_3^{k+1}\|_{FTV} = \mu_3 n_3^{k+1}$, then by using Lipschitz continuous gradient and Young's inequality, the following inequalities for any positive $\{c_i\}_{i=1}^3$ hold

$$\begin{aligned} & \|m_1^{k+1}\|_1 - \|m_1^k\|_1 - \mu_1 \langle n_1^k, m_1^{k+1} - m_1^k \rangle \leq \frac{L_1}{2} \|m_1^{k+1} - m_1^k\|_2^2, \\ & \lambda_1(\|m_2^{k+1}\|_1 - \|m_2^k\|_1) - \mu_2 \langle n_2^k, m_2^{k+1} - m_2^k \rangle \leq \frac{L_2}{2} \|m_2^{k+1} - m_2^k\|_2^2, \\ & \lambda_2(\|m_3^{k+1}\|_{FTV} - \|m_3^k\|_{FTV}) - \mu_3 \langle n_3^k, m_3^{k+1} - m_3^k \rangle \leq \frac{L_3}{2} \|m_3^{k+1} - m_3^k\|_2^2, \\ & -\mu_i \langle m_i^{k+1} - m_i^k, n_i^{k+1} - n_i^k \rangle \leq c_i \mu_i \|n_3^{k+1} - n_3^k\|_2^2 + \frac{\mu_i}{4c_i} \|m_3^{k+1} - m_3^k\|_2^2, \quad i = 1, 2, 3, \end{aligned}$$

if $\{c_i\}_{i=1}^3$ is chosen as $\{\mu_i/2L_i\}_{i=1}^3$, we get

$$\begin{aligned} & L(u^{k+1}, m_1^{k+1}, m_2^{k+1}, m_3^{k+1}, n_1^{k+1}, n_2^{k+1}, n_3^{k+1}) - L(u^k, m_1^k, m_2^k, m_3^k, n_1^k, n_2^k, n_3^k) \\ & \leq \sum_i^3 \left(\frac{L_i}{2} - \frac{\mu_i}{2} + \frac{\mu_i}{4c_i} \right) \|m_i^{k+1} - m_i^k\|_2^2 + (1 + c_i) \mu_i \|n_i^{k+1} - n_i^k\|_2^2 \\ & = \sum_{i=1}^3 C_i \|m_i^{k+1} - m_i^k\|_2^2, \end{aligned}$$

where $C_i = (3L_i - \mu_i)/2 + L_i^2/\mu_i$. Therefore, the first part of the lemma is proved.

b) By using optimality condition for (3.4), there is a $q \in \partial_u(-\lambda_1 \beta_1 \|u\|_2)$ such that

$$\begin{aligned} & q + \mu_1 A^T (Au^{k+1} - f + n_1^k - m_1^k) + \mu_2 W^T (Wu^{k+1} + n_2^k - m_2^k) \\ & + \mu_3 (u^{k+1} + n_3^k - m_3^k) = 0, \end{aligned}$$

now let

$$\begin{aligned} p & = q + \mu_1 A^T (Au^{k+1} - f + n_1^{k+1} - m_1^{k+1}) + \mu_2 W^T (Wu^{k+1} + n_2^{k+1} - m_2^{k+1}) \\ & + \mu_3 (u^{k+1} + n_3^{k+1} - m_3^{k+1}) \in \partial_u L(u^{k+1}, m_1^{k+1}, m_2^{k+1}, m_3^{k+1}, n_1^{k+1}, n_2^{k+1}, n_3^{k+1}), \end{aligned}$$

then we obtain

$$\|p\|_2 \leq \sum_{i=1}^3 c_{i+3}(\mu_i + L_i) \|m_i^{k+1} - m_i^k\|_2, \quad (4.1)$$

where $\{c_i\}_{i=4}^6$ are constant. From the optimality condition of (3.4)-(3.10), the following inequalities for $i = 1, 2, 3$ are obtained

$$\begin{aligned} \|\partial_{m_i} L(u^{k+1}, m_1^{k+1}, m_2^{k+1}, m_3^{k+1}, n_1^{k+1}, n_2^{k+1}, n_3^{k+1})\|_2 &\leq L_i \|m_i^{k+1} - m_i^k\|_2, \\ \|\partial_{n_i} L(u^{k+1}, m_1^{k+1}, m_2^{k+1}, m_3^{k+1}, n_1^{k+1}, n_2^{k+1}, n_3^{k+1})\|_2 &\leq L_i \|m_i^{k+1} - m_i^k\|_2. \end{aligned}$$

Therefore, by combining the above inequalities with (4.1), the relation (b) is obtained. \square

Using the above lemma, the final theorem for convergence is considered as follows. Due to the similarity of the proof with [21], the proof is omitted.

Theorem 4.2. *Considering the assumptions of Lemma 4.1 and let $\mu_i > (3 + \sqrt{17})L_i/2$ for $i = 1, 2, 3$, then*

a) the sequence $(u^k, \{m_i^k\}_{i=1}^3, \{n_i^k\}_{i=1}^3)$ generated by proposed method is bounded and has at least one limit point.

b) $\|u^{k+1} - u^k\|_2 \rightarrow 0$, $\|m_i^{k+1} - m_i^k\|_2 \rightarrow 0$ and $\|n_i^{k+1} - n_i^k\|_2 \rightarrow 0$ for $i = 1, 2, 3$.

c) each limit point $(u^, m_1^*, m_2^*, m_3^*, n_1^*, n_2^*, n_3^*)$ is a stationary point of $L(u, m_1, m_2, m_3, n_1, n_2, n_3)$, and u^* is a stationary point of the proposed model (3.1).*

5 Simulation results

The simulation results of the proposed algorithm that introduced in the previous sections are studied in this section. For simulation results, a computer based on Windows 10-64bit, Intel(R) Core(TM) i3-5005U CPU @2.00GHz, by matlab 2014b is used. Also stopping criterion in this section is considered as

$$\frac{\|u^{k+1} - u^k\|_2}{\|u^{k+1}\|_2} \leq tol,$$

where u^k is the restored image at the k th iteration. In all examples, the tol equal to 10^{-3} is selected. In the analysis of the proposed algorithm various tests including peak signal to noise ratio (PSNR), signal-to-noise ratio (SNR), structural similarity (SSIM), Feature Similarity (FSIM) and Relative Error (ReErr) are studied. More information on these criteria value can be found in [31, 27, 15]. Also ReErr is calculated as

$$ReErr = \frac{\|u^k - u\|_2^2}{\|u\|_2^2}.$$

In the following examples, $M(len, \theta)$ denotes the linear motion blur of a camera by len pixels, with an angle of θ degrees in a counterclockwise direction, $A([r_1, r_2])$ shows the average blur with a size $[r_1, r_2]$, $G(hsize, \sigma)$ denotes the Gaussian blur of size $hsize$ with standard deviation σ (positive).

Example 5.1. (Grayscale image) In this example, Algorithm 1 is used for different images from the USC-SIPI images database¹, i.e., “5.1.12 (256 × 256)”, “5.2.10 (512 × 512)” and “7.1.09 (512 × 512)”. Also “4.2.05” is changed to image with size (256 × 256) by Matlab internal functions and used in the simulation. For images “5.1.12” and “5.2.10”, $A([11, 11])$ with “salt & pepper” and “Random-valued” noise, respectively, with different density are used, for image “7.1.09”, blur kernel $G(7, 4)$ with “salt & pepper” noise with different densities are used. Table 1 compares numerical results for different densities value by proposed algorithm and method in [18]. These results indicate an improvement in the output of the proposed algorithm. Also the blurred and noisy images for “5.2.10” are shown in Figure 1, and the restored images corresponding to each image are given below each image in this figure. Also in order to show the effect of blurred kernel and noise on the image, in Figure 2 (a-d), each of the steps of blurring by $M(35, 135)$ and adding noise by “random-valued” noise with 10% density and restoring image is given separately. In this case we have $PSNR = 33.031$, $SNR = 30.241$, $SSIM = 0.92600$ and $FSIM = 0.99712$. The results in this example show a good representation of the proposed algorithm.

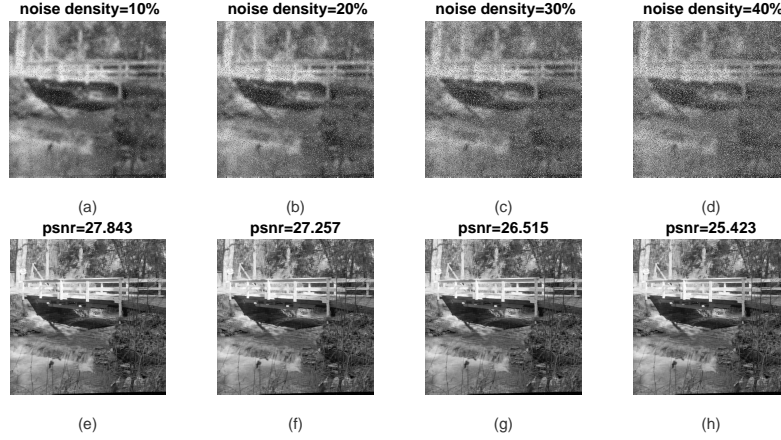


Figure 1: (a-d) Blurred and noisy images, (e-h) restored images for 5.2.10.

Example 5.2. (Color image) In this example, Algorithm 2 is studied for different color images. In the simulation results, “Lena” (512 × 512) image is blurred by following kernel

$$A = \begin{bmatrix} 0.7A([15, 15]) & 0.15G(11, 9) & 0.15G(31, 13) \\ 0.1G(21, 11) & 0.8A([17, 17]) & 0.1A([13, 13]) \\ 0.0M(41, 90) & 0.2M(21, 45) & 0.6M(61, 135) \end{bmatrix},$$

¹<http://sipi.usc.edu/database/>

Table 1: Test results for different grayscale images.

imgae	density	method	PSNR	SNR	ISNR	ReErr	SSIM	FSSIM
5.1.12	10%	Proposed	35.741	33.393	21.702	0.00045781	0.95021	0.9991
		[18]	33.682	31.334	19.55	0.00073556	0.95406	0.9988
	30%	Proposed	28.344	25.995	18.746	0.0025146	0.89537	0.99418
		[18]	27.769	25.421	13.78	0.00287	0.90592	0.99223
5.2.10	10%	Proposed	27.843	21.739	11.106	0.0067000	0.83063	0.99917
		[18]	27.419	21.315	10.654	0.0073876	0.81419	0.99900
	30%	Proposed	26.515	20.411	13.120	0.0090975	0.77559	0.99851
		[18]	26.327	20.223	12.929	0.0094992	0.76804	0.99835
7.1.09	10%	Proposed	33.699	27.89	18.254	0.0016255	0.89393	0.99977
		[18]	33.254	27.445	17.903	0.001801	0.88131	0.99976
	30%	Proposed	32.385	26.576	21.557	0.0021999	0.86585	0.99963
		[18]	31.707	25.898	20.87	0.0025715	0.84426	0.99961

“House” (512×512) image is blurred by

$$A = \frac{1}{3} \text{diag}(A([5, 5]), A([7, 7]), A([9, 9])),$$

blurred kernel for “Peppers” image (256×256) is considered as

$$A = \begin{bmatrix} 0.8A([11, 11]) & 0.1G(11, 5) & 0.1M(21, 135) \\ 0.15A([11, 11]) & 0.7G(11, 5) & 0.15M(21, 135) \\ 0.2A([11, 11]) & 0.2G(11, 5) & 0.6M(21, 135) \end{bmatrix},$$

and finally blurred kernel $A = B \otimes M(41, 135)$ is used for “Plate” with size (256×256), where

$$A = \begin{bmatrix} 0.8 & 0.1 & 0.1 \\ 0.15 & 0.7 & 0.15 \\ 0.2 & 0.2 & 0.6 \end{bmatrix}.$$

Also for the noise process, “salt & pepper” noise is used for “Lena”, “House” and “Plate” images and “random-valued” noise is used for “Peppers” image. Table 2 compares the results of the proposed method with the results of the algorithms in [30] and [20]. Other results are also given in Table 3 for test images. The results show the efficiency of the proposed algorithm in comparison with these algorithms. Also, the proposed algorithm outputs for different images with different noise densities are given in Figures 3-5. Figure 2 (e-h) shows the effect of the blurred kernel and noise on the color image. In this results “salt & pepper” noise with 30% density is used. Test results for this case are included $PSNR = 28.871$, $SNR = 27.049$, $ISNR = 20.636$, $ReErr = 0.0019729$, $SSIM = 0.9535$ and $FSIM = 0.99884$.

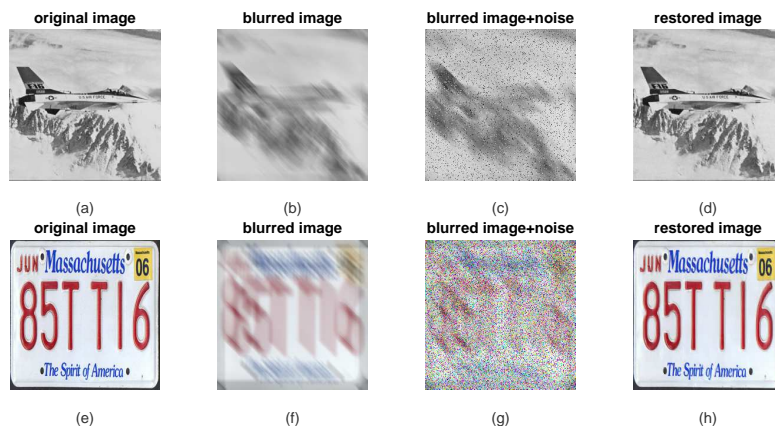


Figure 2: (a,e) Original images, (b,f) blurred images, (c,g) blurred and noisy images, (d,h) restored images.

Table 2: Test results for different color images.

		density		10%		20%		30%		40%	
imgae	method	SNR	SSIM	SNR	SSIM	SNR	SSIM	SNR	SSIM	SNR	SSIM
House	Proposed	27.23	0.9620	26.83	0.9591	26.04	0.9524	24.04	0.9348		
	[30]	22.70	0.9103	22.33	0.9045	22.08	0.9027	21.61	0.8904		
	[20]	25.54	0.9185	24.57	0.9071	23.36	0.9024	22.58	0.8876		
Lena	Proposed	25.15	0.9744	24.96	0.9734	24.66	0.9717	24.33	0.9699		
	[30]	23.50	0.8831	23.48	0.8841	23.87	0.8907	23.71	0.8864		
	[20]	25.12	0.9035	24.48	0.8941	23.88	0.8860	23.90	0.8856		
Peppers	Proposed	26.34	0.9895	25.80	0.9877	24.49	0.9826	20.43	0.9547		
	[30]	22.34	0.8530	21.79	0.8379	20.88	0.8208	19.88	0.7941		
	[20]	23.85	0.8681	22.88	0.8504	21.73	0.8302	20.39	0.7982		

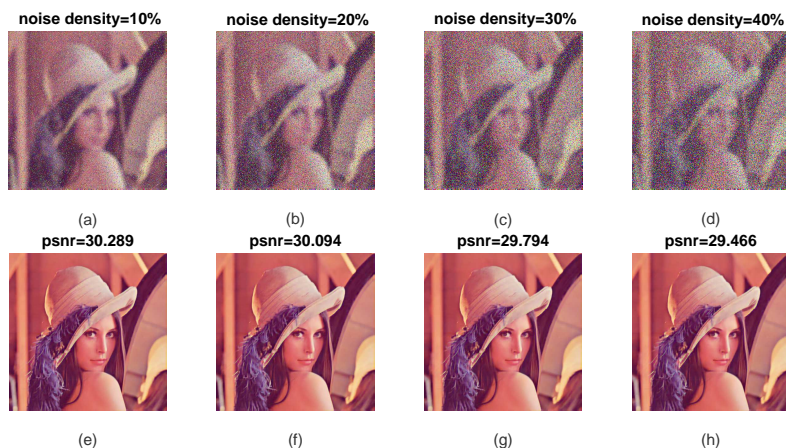


Figure 3: (a-d) Blurred and noisy images, (e-h) restored images for Lena (512×512).

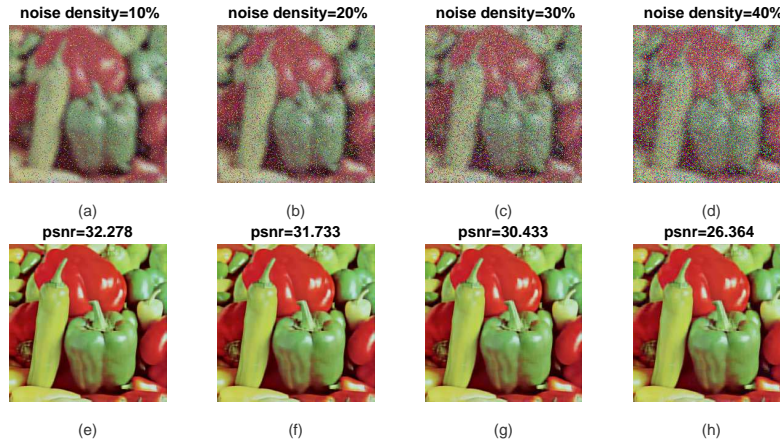


Figure 4: (a-d) Blurred and noisy images, (e-h) restored images for Peppers (256×256).

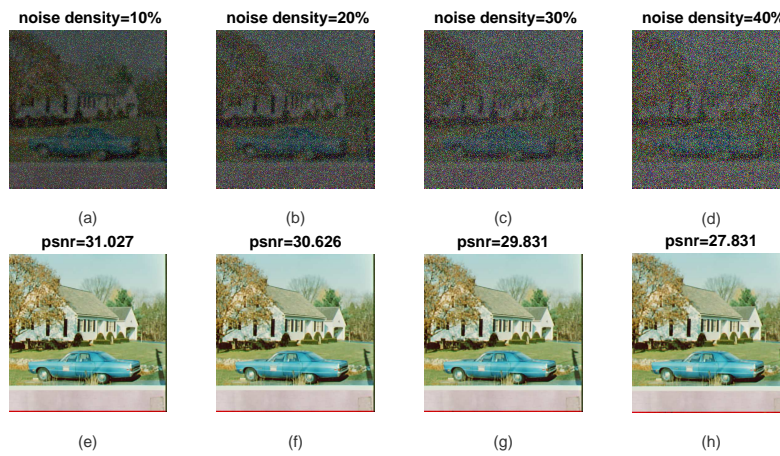


Figure 5: (a-d) Blurred and noisy images, (e-h) restored images for Househ (512×512).

6 Conclusion

In this paper the nonconvex model based on fractional-order total variation and framelet transfer is introduced for image restoration. The proposed model is solved by ADMM and primal-dual methods. In the analysis of the proposed algorithm convergence analysis is studied and simulation results are evaluated. The results have

Table 3: Test results for different grayscale images with different noise densities.

imgae	density	ISNR	ReErr	FSIM
House	10%	24.054	0.0018923	0.99976
	20%	23.907	0.0020754	0.99973
	30%	23.342	0.0024927	0.99965
	40%	21.567	0.0039502	0.99947
Lena	10%	16.234	0.0030536	0.99914
	20%	18.433	0.0031943	0.99908
	30%	19.703	0.0034223	0.99898
	40%	20.507	0.0036912	0.99886
Peppers	10%	16.785	0.0023246	0.99724
	20%	17.983	0.0026354	0.99716
	30%	17.946	0.0035549	0.99689
	40%	14.841	0.0090734	0.99597

been compared with other methods and these results show the efficiency of the proposed algorithm in restoring images that have been damaged due to blur and noise.

References

- [1] Adam, Tarmizi, and Raveendran Paramesran. *Hybrid non-convex second-order total variation with applications to non-blind image deblurring*. Signal, Image and Video Processing 14, no. 1 (2020): 115-123.
- [2] Bioucas-Dias, José M., Mário AT Figueiredo, and Joao P. Oliveira. *Adaptive total variation image deconvolution: A majorization-minimization approach*. In 2006 14th European Signal Processing Conference, pp. 1-4. IEEE, 2006.
- [3] Cai, Jian-Feng, Jae Kyu Choi, Jingyang Li, and Ke Wei. *Image restoration: Structured low rank matrix framework for piecewise smooth functions and beyond*. Applied and Computational Harmonic Analysis 56 (2022): 26-60.
- [4] Cai, Jian-Feng, Stanley Osher, and Zuowei Shen. *Split Bregman methods and frame based image restoration*. Multiscale modeling & simulation 8, no. 2 (2010): 337-369.
- [5] Chen, Scott Shaobing, David L. Donoho, and Michael A. Saunders. *Atomic decomposition by basis pursuit*. SIAM review 43, no. 1 (2001): 129-159.
- [6] De Oliveira, Edmundo Capelas, and José António Tenreiro Machado. *A review of definitions for fractional derivatives and integral*. Mathematical Problems in Engineering 2014 (2014).
- [7] Dong, Bin, Hui Ji, Jia Li, Zuowei Shen, and Yuhong Xu. *Wavelet frame based blind image inpainting*. Applied and Computational Harmonic Analysis 32, no. 2 (2012): 268-279.
- [8] Dong, Fangfang, and Yunmei Chen. *A fractional-order derivative based variational framework for image denoising*. Inverse Problems & Imaging 10, no. 1 (2016): 27.

- [9] Dong, Fangfang, and Qianting Ma. *Single image blind deblurring based on the fractional-order differential*. Computers & Mathematics with Applications 78, no. 6 (2019): 1960-1977.
- [10] Esser, Ernie, Xiaoqun Zhang, and Tony Chan. *A general framework for a class of first order primal-dual algorithms for TV minimization*. Ucla Cam Report 9 (2009): 67.
- [11] Han, Bin. *Framelets and wavelets*. In Algorithms, Analysis, and Applications, Applied and Numerical Harmonic Analysis. Birkhäuser xxxiii Cham, 2017.
- [12] Han, Bin. *Properties of discrete framelet transforms*. Mathematical Modelling of Natural Phenomena 8, no. 1 (2013): 18-47.
- [13] He, Yiyang, Hongli Wang, Lei Feng, and Sihai You. *Motion-blurred star image restoration based on multi-frame superposition under high dynamic and long exposure conditions*. Journal of Real-Time Image Processing 18, no. 5 (2021): 1477-1491.
- [14] Jing, Yu, Jianxin Liu, Zhaoxia Liu, and Hongju Cao. *Fast edge detection approach based on global optimization convex model and split Bregman algorithm*. Diagnostyka 19 (2018).
- [15] Kumar, Rohit, and Vishal Moyal. *Visual image quality assessment technique using fsim*. International Journal of Computer Applications Technology and Research 2, no. 3 (2013): 250-254.
- [16] Li, Bo, and Wei Xie. *Adaptive fractional differential approach and its application to medical image enhancement*. Computers & Electrical Engineering 45 (2015): 324-335.
- [17] Li, Dongming, Changming Sun, Jinhua Yang, Huan Liu, Jiaqi Peng, and Lijuan Zhang. *Robust multi-frame adaptive optics image restoration algorithm using maximum likelihood estimation with poisson statistics*. Sensors 17, no. 4 (2017): 785.
- [18] Liu, Jingjing, Anqi Ni, and Guoxi Ni. *A nonconvex $l_1(l_1-l_2)$ model for image restoration with impulse noise*. Journal of Computational and Applied Mathematics 378 (2020): 112934.
- [19] Liu, Jingjing, Ruijie Ma, Xiaoyang Zeng, Wanquan Liu, Mingyu Wang, and Hui Chen. *An efficient non-convex total variation approach for image deblurring and denoising*. Applied Mathematics and Computation 397 (2021): 125977.
- [20] Liu, Jun, Ting-Zhu Huang, Xiao-Guang Lv, and Jie Huang. *Restoration of blurred color images with impulse noise*. Computers & Mathematics with Applications 70, no. 6 (2015): 1255-1265.
- [21] Lou, Yifei, and Ming Yan. *Fast L_1-L_2 minimization via a proximal operator*. Journal of Scientific Computing 74, no. 2 (2018): 767-785.

- [22] Love, Eric Russell. *Fractional derivatives of imaginary order*. Journal of the London Mathematical Society 2, no. 2 (1971): 241-259.
- [23] Mistakidis, Euripidis S., and Georgios E. Stavroulakis. *Nonconvex optimization in mechanics: algorithms, heuristics and engineering applications by the FEM*. Vol. 21. Springer Science & Business Media, 2013.
- [24] Oliveira, Joao P., José M. Bioucas-Dias, and Mário AT Figueiredo. *Adaptive total variation image deblurring: a majorization–minimization approach*. Signal processing 89, no. 9 (2009): 1683-1693.
- [25] Rudin, Leonid I., Stanley Osher, and Emad Fatemi. *Nonlinear total variation based noise removal algorithms*. Physica D: nonlinear phenomena 60, no. 1-4 (1992): 259-268.
- [26] Sajjad, Muhammad, Irfan Mehmood, Naveed Abbas, and Sung Wook Baik. *Basis pursuit denoising-based image superresolution using a redundant set of atoms*. Signal, Image and Video Processing 10, no. 1 (2016): 181-188.
- [27] Sara, Umme, Morium Akter, and Mohammad Shorif Uddin. *Image quality assessment through FSIM, SSIM, MSE and PSNR—a comparative study*. Journal of Computer and Communications 7, no. 3 (2019): 8-18.
- [28] Shen, Yi, Bin Han, and Elena Braverman. *Image inpainting from partial noisy data by directional complex tight framelets*. The ANZIAM Journal 58, no. 3-4 (2017): 247-255.
- [29] Setzer, Simon. *Split Bregman algorithm, Douglas-Rachford splitting and frame shrinkage*. In International Conference on Scale Space and Variational Methods in Computer Vision, pp. 464-476. Springer, Berlin, Heidelberg, 2009.
- [30] Tao, Min, Junfeng Yang, and Bingsheng He. *Alternating direction algorithms for total variation deconvolution in image reconstruction*. TR0918, Department of Mathematics, Nanjing University (2009).
- [31] Wang, Zhou, Alan C. Bovik, Hamid R. Sheikh, and Eero P. Simoncelli. *Image quality assessment: from error visibility to structural similarity*. IEEE transactions on image processing 13, no. 4 (2004): 600-612.
- [32] Yang, Jingjing, Yingpin Chen, and Zhifeng Chen. *Infrared Image Deblurring via High-Order Total Variation and Lp-Pseudonorm Shrinkage*. Applied Sciences 10, no. 7 (2020): 2533.
- [33] Zhang, Yi, Weihua Zhang, Yinjie Lei, and Jiliu Zhou. *Few-view image reconstruction with fractional-order total variation*. JOSA A 31, no. 5 (2014): 981-995.
- [34] Zhu, Mingqiang, and Tony Chan. *An efficient primal-dual hybrid gradient algorithm for total variation image restoration*. UCLA CAM Report 34 (2008): 8-34.

- [35] Zifan, Ali, and Panos Liatsis. *Medical image deblurring via lagrangian pursuit in frame dictionaries*. In 2011 Developments in E-systems Engineering, pp. 86-91. IEEE, 2011.
- [36] Zou, Jian, Haifeng Li, and Guoqi Liu. *Split Bregman algorithm for structured sparse reconstruction*. IEEE Access 6 (2018): 21560-21569.